Pergamon

0301-9322(94)E0018-E

Int. J. Multiphase Flow Vol. 20, No. 5, pp. 901–913, 1994

0301-9322/94 $7.00 + 0.00

SATURATED CHF IN HORIZONTAL ECCENTRIC ANNULI FOR LOW MASS FLUXES: MEASUREMENT AND MODELLING

J. L. BALIÑO and J. CONVERTI

Comisión Nacional de Energía Atómica, Div. Termohidráulica, Centro Atómico Bariloche, 8400-Bariloche, Río Negro, Argentina

(Received 1 June 1992; in revised form 15 February 1994)

Abstract—Measurements of critical heat flux (CHF) were performed for a horizontal annular channel (diameters 11.2 and 54 mm, approx. 1 m heated length) in which the eccentricity of the inner heater was varied. Measurements for low mass fluxes (up to 1600 kg/m^2/s) using freon-12 at a pressure of approx. 10.3 bar and saturation inlet conditions show a strong influence of eccentricity on CHF. The influence of the mass flux on CHF is only moderate. The data trend is discussed on a basis of the flow pattern under which the phenomenon occurs. A model based on the analysis of an intermittent flow pattern was developed. The model explains satisfactorily the trend of the experimental data.

Key Words: CHF, horizontal flow, eccentric annuli, intermittent flow

1. INTRODUCTION

The magnitude of heat transfer rates which can be achieved in two-phase boiling systems is limited by the boiling crisis phenomenon. The ability to predict the CHF phenomenon is essential in the design and safety analysis of installations like boilers or nuclear fuel channels.

Among the huge amount of data, very few correspond to horizontal channels. Differences can be expected between horizontal and vertical CHF because of the transversal gravity force present in horizontal flow. This force tends to stratify the flow, with the lighter phase at the top of the channel; on the other hand, turbulent mixing tends to homogenize the phase distribution.

Due to the buoyancy force, different flow patterns (namely stratified, wavy, bubble elongated and horizontal slug) appear in horizontal flow. When the gas or liquid superficial velocity is high enough, the importance of the buoyancy force decreases, resulting in similar flow patterns for horizontal and vertical flows.

Merilo (1977) reviewed early works done on CHF in horizontal and vertical tubes and rod bundles. With the available data and additional experiments for horizontal and vertical tubes using water and freon-12 in similar conditions (Merilo & Ahmad 1979), it was concluded that horizontal and vertical CHF values are essentially identical for mass fluxes greater than approx. 4000 kg/m^2/s; below this value, CHF was found to be lower for horizontal channels.

The stratification effects are responsible for the high circumferential anisothermality measured by many investigators (Bar-Cohen *et al.* 1983; Kefer *et al.* 1989) and for premature dryout at low flows (Fisher *et al.* 1978).

Bar-Cohen *et al.* (1983) reviewed horizontal boiler-tube data and made an analysis based on operating lines drawn on a flow pattern map. The high temperature differences between thermocouples located at the top and bottom of heated tubes were attributed to the occurrence of a stratified or intermittent flow pattern, showing that the top surface dried for very low qualities. The magnitude of the temperature difference was influenced by circumferential heat conduction effects through the pipe wall.

Experimental data for eccentric annular channels are scarce. Levy *et al.* (1962) performed CHF experiments for vertical eccentric annuli using water and found no influence of eccentricity on CHF. Tolubinskii *et al.* (1971) conducted CHF experiments for a wide range of variables using water in vertical eccentric annuli and also found no influence of eccentricity on CHF.

Modelling of the CHF phenomenon and correlation of the experimental data has been focused on the different flow-patterns which appear in the channel (Kutateladze & Leontiev 1966; Tong 1972; Fiori & Bergles 1970; Hewitt 1982).

Wong *et al.* (1990) compiled CHF data from several sources and developed a generalized CHF prediction method for horizontal tubes, based on a modification of the vertical data by using a correction factor. This correction factor was determined semiempirically using the flow-pattern map developed by Taitel & Dukler (1986). The correction factor given by Wong *et al.* is 0 for any condition in stratified flow and changes to 1 for homogeneous annular or dispersed flow, which shows that a strong heat transfer deterioration occurs at low flows.

The occurrence of different flow patterns seems to be a reasonable explanation for differences in horizontal and vertical CHF. For instance, the threshold mass flux value of 4000 kg/m^2/s reported by Merilo (1977) corresponds roughly to the limit between intermittent and dispersed regimes in a typical horizontal flow-pattern map.

The objective of this work is to study the CHF phenomenon in a horizontal annular channel in which it is possible to change the eccentricity of the inner heater. The experiments were carried out using freon-12 as coolant.

2. APPARATUS AND PROCEDURE

2.1. Freon-12 loop

A simplified schematic diagram of the freon-12 loop used in the experiments is shown in figure 1 (Baliño *et al.* 1989). Subcooled freon-12 coming from the pump was heated in the preheaters; the inlet temperature was controlled by regulating the power released in the preheaters. The test section inlet pressure was adjusted by controlling pressure in a pressurizer. The test section flow rate was adjusted by means of a throttling valve. The maximum operational parameters of the loop are shown in table 1.

2.2. Test section

The test section consisted of an annular channel; the tube inner diameter was $D = 54$ mm. The heater was a thin-walled SS 304 L tube (outer diameter $d = 11.2$ mm, 0.25 mm wall thickness, heated length $L \simeq 1$ m).

The heater was instrumented with ten chromel–alumel thermocouples placed at the wall inner side, in such a way that it was possible to monitor the temperatures at the top and bottom levels of the heater in five different axial locations uniformly spaced; after this, the inner space was filled with cement to prevent collapse under external pressure.

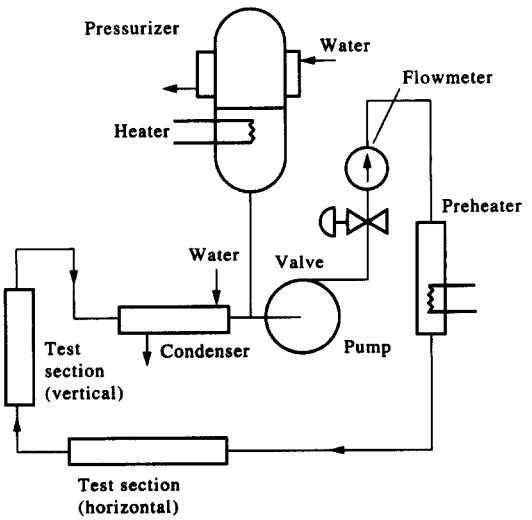

Figure 1. Schematic diagram of the freon-12 loop.

Table 1. Maximum operational parameters of the freon-12 loop

Maximum operating pressure	25 bar
Design pressure	31 bar
Maximum mass flowrate	14,000 kg/h
Maximum heating power	50 kW

Table 2. Range of variables explored in the experiments

Inlet pressure	approx. 10.3 bar
Mass flux	240–1600 kg/m^2/s
Inlet temperature	approx. 41.8°C (saturation)
Tube diameter	54 mm
Heater diameter	11.2 mm
Heated length	1012 mm
Eccentricity	−15 to 15 mm from the concentric position

The heater electrical resistance was approx. 83 mΩ and was heated with a 50 kW d.c. power supply. By means of two positioners, it was possible to change the eccentricity.

Power in the test section was determined by measuring the voltage drop across the test section and across a shunt resistance built in the power source. The inlet pressure was measured with a DP-cell, while the test section flow rate was monitored with a turbine flowmeter. The thermocouple outputs were monitored with digital thermometers.

2.3. CHF detection

CHF detection was performed by measuring the voltage unbalance signal from a resistance bridge (Baliño & Mendieta 1989). The signal was proportional to the difference of electrical resistances of the two halves of the heater, due to temperature changes, as the power was increased. This method has the following advantages:

- High response speed, which is important for CHF in subcooled conditions.
- It is not necessary to know the exact location of the hot patch, which makes it suitable for CHF experiments with non-uniform power distributions and spacer grids.
- Although the resulting wall temperatures obtained when CHF occurred were not high enough (approx. 300°C) to destroy the heater, it is important to limit them when organic refrigerants like freon-12 are used, because these decompose at lower temperatures, thus altering the surface conditions.

The measurements were performed by maintaining the test section inlet pressure, inlet temperature and flow constant; a slow power ramp was set and the resistance bridge was manually balanced until CHF caused a sudden and sharp unbalance signal. When the absolute value of this signal exceeded a preset value, power was automatically cut off.

In many occasions, the power cutoff signal and a sudden increase in some thermocouple signals were detected simultaneously, but there were cases in which the dry patch appeared first in regions where the wall temperature was not measured.

The range of variables explored is given in table 2.

3. EXPERIMENTAL RESULTS AND DISCUSSION

The experimental results are shown in figure 2 (Baliño & Converti 1991) and in table 3. Eccentricity is measured in terms of the length the heater is displaced from its concentric position, eccentricity being positive when the heater is displaced upwards.

CHF decreases sharply as the heater is displaced upwards from its concentric position, and remains constant (or even decreases slightly) as it moves downwards.

The influence of mass flux on the maximum CHF value is only moderate, and the main effect is flattening the CHF vs eccentricity profile. This agrees with the role of turbulence as a mixing agent.

For each condition CHF was measured twice; it can be seen that CHF data showed good repeatability, though a trend to deteriorate this nature is observed at some points with mass flux $G = 243$ kg/m^2/s. Considering that pressure changed slightly for different points, it seems to be that the data corresponding to the lowest mass flux are more sensitive to pressure variations around the mean value.

An explanation for the data trend can be obtained by calculating the superficial velocities for the liquid and gas phase (correspondingly V_{SL} and V_{SG}) at the exit of the test section, based on

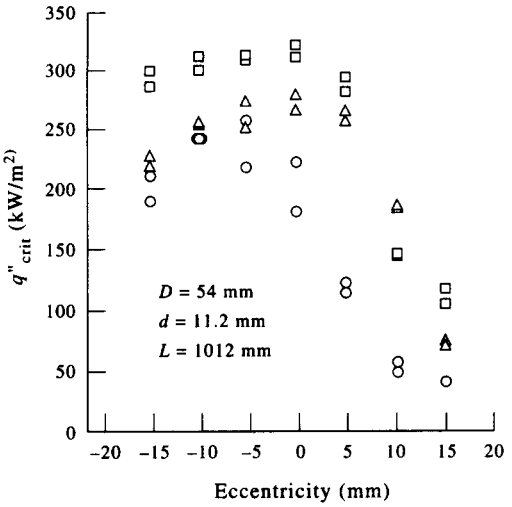

Figure 2. CHF as a function of eccentricity (mean values and standard deviations are shown between parentheses). $p = (10.3 \pm 0.4)$bar; $T_{IN} = (41.8 \pm 0.7)$°C; ○, $G = (243 \pm 3)$kg/m^2/s; △, $G = (788 \pm 5)$kg/m^2/s; □, $G = (1576 \pm 8)$kg/m^2/s.

Table 3. Experimental data

Eccentricity (mm)	p (bar)	T_{IN} (°C)	G (kg/m^2/s)	q''_{CRIT} (kW/m^2)
15	10.5	41.8	247	40.9
15	10.5	42.2	245	40.3
10	9.71	41.4	238	48.8
10	9.68	41.4	239	56.9
5	9.92	41.9	241	114
5	10.1	41.8	241	120
0	9.94	42.5	242	181
0	10.9	41.5	243	222
−5	9.70	41.4	244	218
−5	10.6	41.9	247	257
−10	11.1	41.5	244	242
−10	10.1	41.9	248	241
−15	10.3	41.1	245	212
−15	11.1	41.2	244	191
−15	9.87	41.9	795	227
−15	11.0	41.4	794	219
−10	10.1	42.5	780	255
−10	10.9	41.5	783	253
−5	9.86	41.9	784	252
−5	10.9	42.3	788	271
0	10.2	43.0	790	266
0	10.6	42.7	783	279
5	10.3	42.9	786	256
5	10.5	43.5	786	265
10	10.9	42.2	783	183
10	10.9	42.0	788	185
15	9.96	40.1	792	68.6
15	10.1	40.1	795	72.9
15	9.96	41.9	1576	115
15	9.87	41.8	1581	103
10	9.98	42.4	1589	146
10	9.98	42.5	1571	144
5	9.73	41.5	1572	281
5	10.1	42.6	1559	291
0	11.0	40.7	1575	320
0	10.1	41.6	1583	311
−5	10.6	41.3	1570	313
−5	10.6	41.4	1573	309
−10	9.99	42.1	1589	299
−10	10.3	42.3	1582	311
−15	11.1	41.0	1571	297
−15	10.2	41.6	1572	286

a mass and energy balance with the assumption of one-dimensional flow, saturation inlet conditions and thermodynamic equilibrium:

$$V_{SL} = \frac{G}{\rho_L}\left(1 - \frac{\dot{Q}_{CRIT}}{A_S G h_{LG}}\right) \quad [1]$$

$$V_{SG} = \frac{\dot{Q}_{CRIT}}{\rho_G A_S h_{LG}} \quad [2]$$

where $A_S = \pi/4(D^2 - d^2)$ is the passage area, $\dot{Q}_{CRIT}$ is the total heat power at the CHF condition, ρ_L and ρ_G are correspondingly the liquid and gas densities and h_{LG} is the phase-change enthalpy.

In figure 3 the calculated superficial velocities are shown in a typical horizontal flow-pattern map (Mandhane *et al.* 1974); although this map was built for air–water mixtures flowing in horizontal tubes under fully developed conditions, qualitative similar information was obtained for rod bundles (Osamusali *et al.* 1991) and for two-phase freon-12 flow (Hashizume 1983). It can be seen that the data points fall in the intermittent flow region (bubble elongated or horizontal slug). The data corresponding to $G = 243$ kg/m^2/s are close to the stratified-to-intermittent flow-pattern transition; this could possibly be the reason for the deterioration repeatability observed in these data.

Assuming that CHF occurs under an intermittent flow pattern, the position of the heater will limit the liquid height at the tail of the gas pockets. Therefore, CHF should depend strongly on the dynamics of gas pockets in horizontal intermittent flows. This assumption is supported by the following experimental facts:

- Except for some cases in which the heater was placed close to the bottom of the test section, CHF was detected first by the thermocouples located at the top level of the heater. This suggests dryout as the mechanism responsible for CHF.
- Although in most of the cases CHF was detected at the heater downstream portion, in some cases (when the heater was placed close to the top of the test section and for low mass fluxes) CHF occurred at the upstream portion. There were also cases in which measurements were repeated and CHF was detected at the downstream as well as the upstream portion of the heater, with no significant differences in the CHF values obtained. This indicates a phenomenon of unsteady nature.

4. PHYSICAL MODEL

The main hypotheses of the model are (Baliño 1991):

- CHF occurs under an intermittent flow pattern.
- The postulated CHF mechanism is dryout in a situation where the liquid level under the gas pockets reaches the heater top level. This assumption implies that the power required to evaporate the liquid film that covers the heater top surface during passage of the gas pockets is negligible compared to the total power needed to establish the intermittent flow pattern in the channel. This statement is in agreement with experiments in which premature dryout was observed in horizontal tubes (Bar-Cohen *et al.* 1983).

The gas pockets grow as they move along the test section; we assume that the hydrodynamic parameters calculated hereafter correspond to the channel exit.

4.1. Analysis of the gas pockets in a horizontal eccentric annular channel

A gas pocket is idealized as shown in figure 4; it has length l_F and moves with velocity C. The liquid velocity in front of the gas pocket is $u_S < C$.

The liquid height at the tail of a gas pocket is h_1, which will be coincident with the heater top level when CHF occurs. The length of the liquid region between two successive gas pockets is l_S. The gas pocket unit length l_U is defined as $l_U = l_F + l_S$.

Aeration outside the gas pockets and acceleration effects are neglected; it is assumed that the vapor generated by the boiling process instantaneously feeds the gas pockets. Besides, pressure variations inside the gas phase are negligible, i.e. the gas pockets are treated as constant pressure cavities.

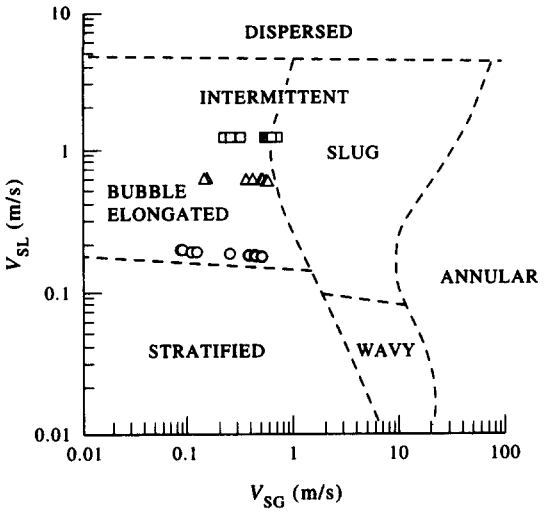

Figure 3. Experimental superficial velocities in a typical horizontal flow pattern map (mean values and standard deviations are shown in parentheses). $p = (10.3 \pm 0.4)$bar; $T_{IN} = (41.8 \pm 0.7)$°C; ○, $G = (243 \pm 3)$kg/m²/s; △, $G = (788 \pm 5)$kg/m²/s; □, $G = (1576 \pm 8)$kg/m²/s.

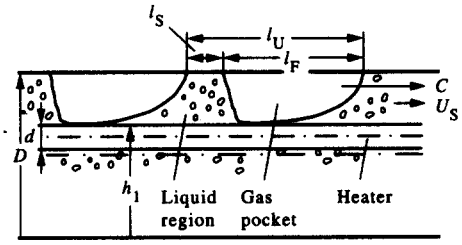

Figure 4. Idealization of a gas pocket.

4.1.1. Necessary conditions derived from the analysis of the tail of a gas pocket. Considering the control volume shown in figure 5 in a reference frame moving with velocity C, assuming one-dimensional flow and neglecting shear stresses at the walls, the continuity and momentum conservation equations reads (Ruder *et al.* 1989; Ruder & Hanratty 1990):

$$(C - u_l)A_l = (C - u_S)A_S \quad [3]$$

$$\int_{A_S} p \, dA - \int_{A_l} p \, dA = \rho_L (C - u_l)^2 A_l (1 - A_l/A_S) \quad [4]$$

where A_l and u_l are correspondingly the area and the velocity of the liquid phase at the tail of the gas pocket.

The pressure distributions in sections 1 and S are

$$p(z) = \rho_L g(h_l - z) \quad [5]$$

$$p_S(z) = \Delta p + \rho_L g (D - z) \quad [6]$$

where Δp is the pressure difference between the upper point of section S and any point within the gas pockets. Considering an isoentropic evolution between these two points, the following relationship (namely Bernoulli equation) holds

$$\Delta p_{REV} + \tfrac{1}{2}\rho_L (C - u_S)^2 + \rho_L g D = \tfrac{1}{2}\rho_L (C - u_l)^2 + \rho_L g h_l \quad [7]$$

According to the second principle of thermodynamics

$$\Delta p_{REV} \geqslant \Delta p \quad [8]$$

Calculating the net pressure force and using [3], [4], [7] and [8], a necessary condition for the existence of gas pockets of height h_l can be derived.

In a non-dinemsional form and taking D, u_S and $\pi D^2/4$ correspondingly as reference length, velocity and area, this condition results

$$(C^* - 1)\mathrm{Fr}_S \geqslant \frac{A_l^*}{1 - d^{*2}} \phi_l \quad [9]$$

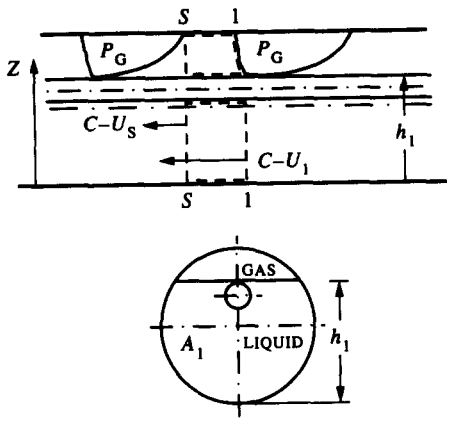

Figure 5. Control volume at the tail of the gas pocket.

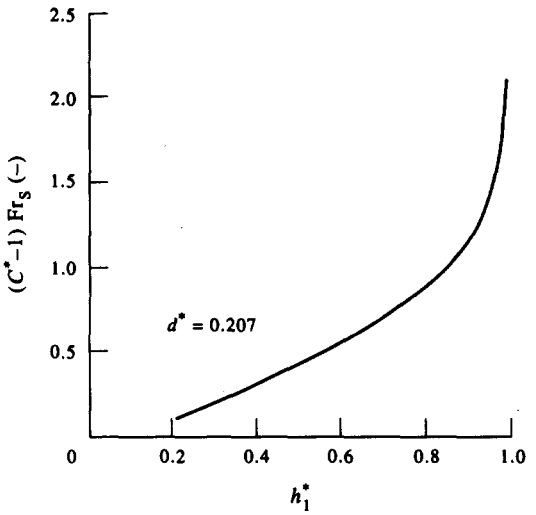

Figure 6. Propagation velocity of the gas pockets.

where $Fr_S = u_S/(gD)^{1/2}$ is the reference Froude number, $\phi_1 = (h_1^*, d^*)$ and

$$\phi(h^*, d^*) = \frac{\frac{8}{3\pi}[h^*(1-h^*)]^{3/2} - 1/2[1-d^{*2} - A^*(2h^*-1)] + (1-h^*)(1-d^{*2})}{1/2(1-d^{*2})\left[1-\left(\frac{A^*}{1-d^{*2}}\right)^2\right] - A^*\left(1-\frac{A^*}{1-d^{*2}}\right)}^{1/2} \quad [10]$$

The non-dimensional area A^* can be calculated as

$$A^* = \frac{1}{\pi}\left[2(2h^*-1)\sqrt{h^*(1-h^*)} + \arcsin(2h^*-1) + \frac{\pi}{2} - \pi d^{*2}\right] \quad [11]$$

The departure of the equality in [9] will be larger as dissipation at the hydraulic jump at the tail of a gas pocket becomes important. Because of the low reference Froude numbers involved ($0.4 \leqslant Fr_S \leqslant 2.7$) it is assumed that the influence of energy losses can be neglected. Thus, equality in [9] is used to determine the velocity of the gas pockets.

$$(C^*-1)Fr_S = \frac{A_1^*}{1-d^{*2}}\phi_1 \quad [12]$$

This relationship is shown in figure 6, as a function of the non-dimensional liquid height at the tail of a gas pocket. It can be observed that $(C^*-1)Fr_S$ increases as h_1^* increases. Besides, C^* is always greater than unity and tends to unity as the liquid height tends to zero.

4.1.2. Analysis of the shape of a gas pocket. In reference frame moving with a velocity C, a control volume shown in figure 7 is considered. This control volume has thickness dx and comprises the liquid under a gas pocket.

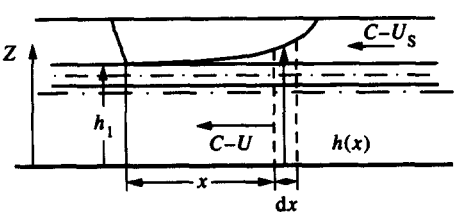

Figure 7. Control volume comprising the liquid under a gas pocket.

The shape of a gas pocket is determined by applying conservation of mass and momentum for one-dimensional flow (Dukler & Hubbard 1975):

$$\frac{\mathrm{d}}{\mathrm{d}x}[(C-u)A]=0 \Rightarrow (C-u)A=(C-u_S)A_S \quad [13]$$

$$\tau_W \mathscr{P}+\frac{\mathrm{d}}{\mathrm{d}x}\left(\int_A p\,\mathrm{d}A\right)=\rho_L\left[(C-u_S)\frac{A_S}{A}\right]^2\frac{\mathrm{d}A}{\mathrm{d}x} \quad [14]$$

where u is the liquid mean velocity at position x.

The mean wall shear stress τ_W is calculated using a friction factor f based on a local Reynolds number with the hydraulic diameter D_H:

$$f(\mathrm{Re}_{D_H})=\frac{4\tau_W}{1/2\rho_L u^2} \quad [15]$$

$$\mathrm{Re}_{D_H}=\frac{uD_H}{\nu_L} \quad [16]$$

$$D_H=\frac{4A}{\mathscr{P}} \quad [17]$$

where $\mathscr{P}$ is the local wetted perimeter.

A known correlation which closely fits the Karman–Nikuradse equation for smooth pipes in the range $3\times10^4<\mathrm{Re}_{D_H}<10^6$ (Kays & Crawford 1980) is used to calculate the friction factor:

$$f=0.184(\mathrm{Re}_{D_H})^{-0.20} \quad [18]$$

A hydrostatic pressure variation is assumed for the control volume:

$$p(z)=\rho_L g(h-z) \quad [19]$$

In a non-dimensional form, the following relationships hold:

$$\mathscr{P}^*=\arccos(1-2h^*)+\pi d^* \quad [20]$$

$$D_H^*=\pi A^*/\mathscr{P}^* \quad [21]$$

$$\mathrm{Re}_{D_H}=u^* D_H^*\,\mathrm{Re}_S \quad [22]$$

where $\mathrm{Re}_S=u_S D/\nu_L$ is the reference Reynolds number.

Calculating the net pressure force in the control volume, and considering

$$\frac{\mathrm{d}}{\mathrm{d}x^*}=\frac{\mathrm{d}h^*}{\mathrm{d}x^*}\frac{\mathrm{d}}{\mathrm{d}h^*} \quad [23]$$

the variation of the liquid height with respect to position is obtained:

$$\frac{\mathrm{d}h^*}{\mathrm{d}x^*}=\frac{\frac{1}{2\pi}f\mathscr{P}^*\left\{\mathrm{Fr}_S\left[C^*-\frac{(C^*-1)(1-d^{*2})}{A^*}\right]\right\}^2}{\left[\frac{\mathrm{Fr}_S(C^*-1)(1-d^{*2})}{A^*}\right]^2\frac{\mathrm{d}A^*}{\mathrm{d}h^*}-\frac{\mathrm{d}}{\mathrm{d}h^*}\left(\int_{A^*}p^*\,\mathrm{d}A^*\right)} \quad [24]$$

It can be easily shown that

$$\frac{\mathrm{d}A^*}{\mathrm{d}h^*}=8/\pi\sqrt{h^*(1-h^*)} \quad [25]$$

$$\frac{\mathrm{d}}{\mathrm{d}h^*}\left(\int_{A^*}p^*\,\mathrm{d}A^*\right)=A^* \quad [26]$$

Replacing [12] and [26] in [24] it is finally obtained

$$\frac{\mathrm{d}h^*}{\mathrm{d}x^*}=\frac{\frac{1}{2\pi}f\mathscr{P}^*\left[\mathrm{Fr}_S-\phi_1 A_1^*\left(\frac{1}{A^*}-\frac{1}{1-d^{*2}}\right)\right]^2}{\left(\frac{A_1^*}{A^*}\phi_1\right)^2\frac{\mathrm{d}A^*}{\mathrm{d}h^*}-A^*} \quad [27]$$

The length of the gas pocket is calculated by integrating [27] between points $(x^* = 0, h^* = h_l^*)$ and $(x^* = l_F^*, h^* = h_\infty^*)$ such that

$$\left(\frac{A_l^*}{A_\infty^*}\phi_l\right)^2 \frac{dA^*}{dh^*}(h_\infty^*) - A_\infty^* = 0 \qquad [28]$$

For $h^* \to h_\infty^*$, $dh^*/dx^* \to \infty$ and, according to the model, the nose of the gas pocket becomes perpendicular to the flow direction. In the region close to the nose of the gas pocket the assumption of one-dimensional flow is no longer valid (Benjamin 1968).

An interesting derivation regarding a necessary condition for existence of gas pockets of height h_l^* can be obtained from [27]. According to the model, it is necessary that the absolute liquid velocity be positive for a gas pocket to exist. Otherwise, dh^*/dx^* would not be positive and integration of [27] could not be performed. From [27] the condition of positive liquid velocity is equivalent to

$$Fr_S - \phi_l A_l^* \left(\frac{1}{A^*} - \frac{1}{1 - d^{*2}}\right) > 0 \qquad [29]$$

From [29], a minimum reference Froude number can be determined, below which a gas pocket of height h_l^* cannot exist:

$$Fr_S > (Fr_S)_{MIN} = \phi_l \left(1 - \frac{A_l^*}{1 - d^{*2}}\right) \qquad [30]$$

In figure 8 is shown the minimum Froude number as a function of the non-dimensional liquid height at the tail of a gas pocket. It can be seen that $(Fr_S)_{MIN}$ increases as h_l^* decreases; this is in agreement with the experimental evidence (Dukler & Hubbard 1975; Ruder & Hanratty 1990; Kvernvold *et al.* 1984) that for a fixed liquid superficial velocity a greater gas superficial velocity is needed to obtain gas pockets with thinner liquid films. In this figure the Froude numbers calculated from the experimental data are also shown; it can be seen that the experimental data fulfill the necessary condition [30].

According to [27]:

$$h^* = h^*(x^*, h_l^*, Fr_S, Re_S, d^*) \qquad [31]$$

$$l_F^* = l_F^*(h_l^*, Fr_S, Re_S, d^*) \qquad [32]$$

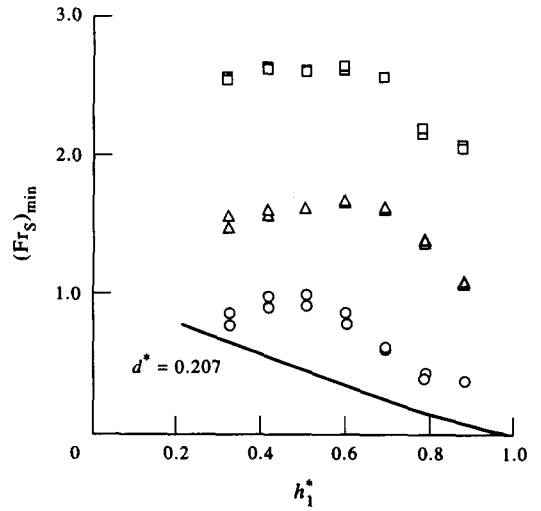

Figure 8. Minimum Froude number derived from the analysis of the shape of a gas pocket (mean values and standard deviations are shown in parentheses). $p = (10.3 \pm 0.4)$bar; $T_{IN} = (41.8 \pm 0.7)$°C; ○, $G = (243 \pm 3)$kg/m²/s; △, $G = (788 \pm 5)$kg/m²/s; □, $G = (1576 \pm 8)$kg/m²/s.

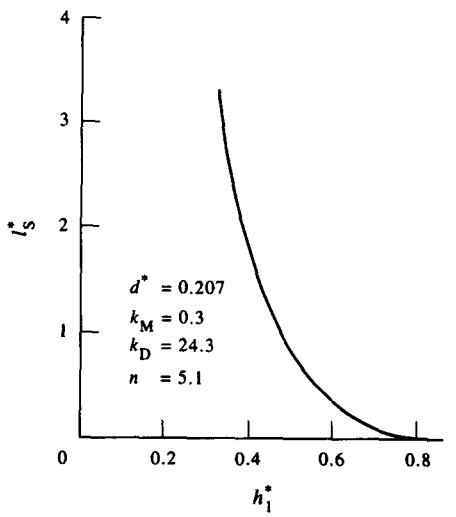

Figure 9. Length of the liquid region as a function of the liquid height at the tail of a gas pocket.

4.1.3. Determination of hydrodynamic parameters.

Volume of the gas pockets: the non-dimensional volume of a gas pocket $\mathscr{V}_G^*$ can be easily obtained as

$$\mathscr{V}_G^* = \frac{4\mathscr{V}_G}{\pi D^3} = (1 - d^{*2})l_F^* - \int_0^{l_F^*} A^* \, dx^* \quad [33]$$

Frequency of the gas pockets: the frequency of passage of the gas pockets ν_U can be calculated as

$$\nu_U = \frac{C}{l_U} = \frac{C}{l_F + l_S} \quad [34]$$

Mass flowrates: the average gas mass flowrate $\dot{m}_G$ can be easily calculated as

$$\dot{m}_G = \rho_G \mathscr{V}_G \nu_U = \frac{\rho_G \mathscr{V}_G C}{l_F + l_S} \quad [35]$$

For the average liquid mass flowrate $\dot{m}_L$, the liquid region and the liquid under a gas pocket must be considered, resulting in

$$\dot{m}_L = \frac{\rho_L}{l_F + l_S}[u_S A_S (l_F + l_S) - C\mathscr{V}_G] \quad [36]$$

Superficial velocities: from [35] and [36], the superficial velocities for the liquid and gas phases can be calculated as

$$V_{SL} = \frac{\dot{m}_L}{\rho_L A_S} = u_S - \frac{C\mathscr{V}_G}{(l_F + l_S)A_S} \quad [37]$$

$$V_{SG} = \frac{\dot{m}_G}{\rho_G A_S} = \frac{C\mathscr{V}_G}{(l_G + l_S)A_S} \quad [38]$$

The velocity in the liquid region at the front of a gas pocket can be obtained by adding [37] and [38]:

$$u_S = V_{SL} + V_{SG} \quad [39]$$

Length of the liquid region: to complete the model it is necessary to determine the length of the liquid region.

The experiments with horizontal pipes in which the length of the liquid region was measured (Ruder & Hanratty 1990; Kvernvold *et al.* 1984; Nicholson *et al.* 1978) dealt with "stable" or "fully developed" intermittent flows, i.e. flows in which two successive gas pockets do not coalesce. In these experiments, a length of the order of 200 diameters was left between the fluid injection and measuring locations. The length of liquid regions reported ranged form 12 to 30 diameters.

It can be considered that the length of the liquid region comprises a mixing length and a developing length (Dukler *et al.* 1985).

The mixing length is associated with the acceleration of the low velocity liquid at the tail of a gas pocket by the high velocity liquid at the front of the successive gas pocket. This momentum interchange originates a mixing vortex.

The developing length is associated with the length of time the flow takes to develop, once the boundary layer is disturbed or distorted by the mixing vortex.

In fully developed intermittent flows, the mixing length is small compared to the developing length. In the present model, the mixing length l_M is considered to be proportional to the head loss in a sudden expansion from area A_1 to A_S. In a non-dimensional form, this results (Potter & Foss 1975)

$$l_M^* = 1/2K_M \, Fr_S^2 (1 - u_1^*)^2 \quad [40]$$

It is assumed $K_M = 0.3$ (Dukler & Hubbard 1975).

In the CHF experiments, the continuous vapor generation and the comparatively short length of the test section indicates a situation far away from the stable condition. In the literature there is no analysis of the liquid length for non-stable intermittent flows. It is assumed here that the developing length l_D is only a function of the height of the liquid under the gas pockets:

$$l_D^* = l_D(h_1^*) = K_D(1 - h_1^*)^n \quad [41]$$

where K_D and n are constants adjusted from the experimental data ($K_D = 24.3$, $n = 5.1$).

The length of the liquid region can be obtained as

$$l_S^* = l_M^* + l_D^* \quad [42]$$

It is important to realize that according to [12], [13], [40], [41] and [42] the length of the liquid region is only a function of h_ℓ^* and d^*. The final result is

$$l_S^* = 1/2K_M\phi_\ell^2\left(1 - \frac{A_\ell^*}{1 - d^{*2}}\right)^2 + K_D(1 - h_\ell^*)^n \quad [43]$$

The length of the liquid region as a function of the non-dimensional liquid height at a tail of a gas pocket is shown in figure 9. It is observed that there is a strong influence of h_ℓ^* on l_S^*; besides, the resulting liquid lengths are shorter than the ones reported in experiments for horizontal intermittent flows under stable conditions.

4.2. Calculation scheme

The main result obtained from the model is the vapor superficial velocity that allows a gas pocket of height h_ℓ^* to exist at the exit of the test section, maintaining a constant mass flux G. An iterative method is required, because the gas and liquid superficial velocities determine u_S, which in turn modifies the reference Reynolds and Froude numbers.

Once the hydrodynamic problem is solved, the critical power and CHF can be calculated from [2]:

$$\dot{Q}_{CRIT} = \rho_G A_S h_{LG} V_{SG} \quad [44]$$

$$q''_{CRIT} = \frac{\dot{Q}_{CRIT}}{\pi\, dL} \quad [45]$$

5. DISCUSSION OF RESULTS

In figure 10 the CHF experimental data are plotted against the values calculated by using the model, for the same thermalhydraulic conditions (mass flux, pressure and eccentricity). According to [44] and [45], the CHF is proportional to the gas superficial velocity.

It can be observed that the model explains satisfactorily the data trend with respect to eccentricity and the moderate influence of the mass flux. Physically, as the velocity u_S is increased, the gas pockets move faster but have shorter lengths, resulting in a moderate influence of the mass flux on CHF.

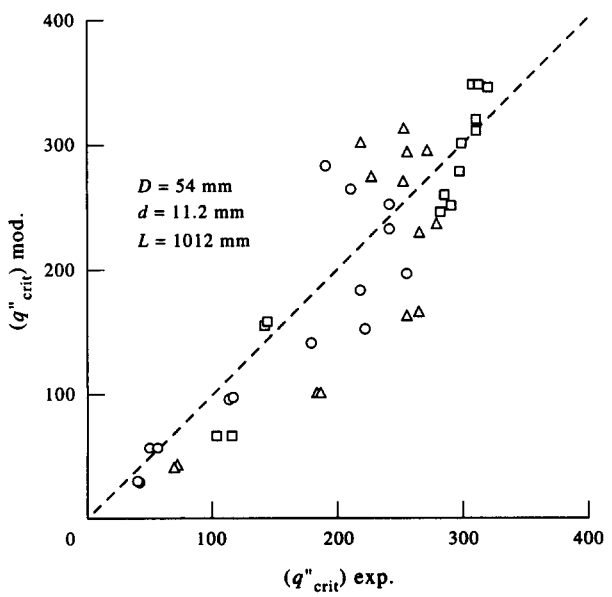

Figure 10. Comparison between experimental and predicted data.

For the situations in which the heater is close to the top of the test section, the model tends to underpredict the experimental data. This is probably due to the fact that aereation was not taken into account; aereation should be important as the fraction of the cross-sectional area accupied by the gas pockets diminishes. Another explanation could be that when the heater is close to the top of the test section, the power required to evaporate the liquid film that covers the heater top surface during passage of the gas pockets becomes important compared to the total power.

For situations in which the heater is close to the bottom of the test section, the model tends to overpredict the experimental data. Probably there is a competing mechanism, by which a departure of nucleate boiling occurs at the tail of a gas pocket, where the absolute liquid velocity is minimum. In some cases, when the heater was positioned close to the bottom of the test section, CHF was also detected by the thermocouples located at the bottom level of the heater. This mechanism resembles the one reported by Bergles (1977) for vertical slug flow patterns.

Due to the simplicity of the model, the upstream effect on CHF could not be explained, but this does not invalidate the main assumptions. Additional experiments would be required to study the influence of the above-mentioned effects on CHF.

6. CONCLUSIONS

Measurements for a horizontal annular channel (diameters 11.2 and 54 mm, approx. 1 m heated length) using freon-12 with saturation inlet conditions at approx. 10.3 bar, show a strong influence of eccentricity on CHF. This influence is important for the safety analysis in horizontal channels of nuclear reactors such as CANDU.

The influence of mass flux (up to 1600 $kg/m^2/s$) on CHF is only moderate.

A model based on the dynamics of horizontal intermittent flows has been developed, which explains satisfactorily the data trend. The limitations of the model have to do with the lack of basic knowledge about intermittent flow patterns under non-stable conditions and boiling. Additional detailed experiments have to be performed to study the problem. Some of these experiments are being carried out at our laboratory.

This work aims to verify the close relationship between the CHF mechanism and the flow pattern in the channel.

Acknowledgements—The financial support for this work was provided by the Comisión Nacional de Energia Atómica and the International Atomic Energy Agency. The contribution of D. Mateos and M. Enevoldsen in building the test section is greatly acknowledged.

REFERENCES

BALIÑO, J. L., CONVERTI, J. & RUIVAL, M. H. 1989 Descripción del circuito de freón 12 en el laboratorio de Termohidráulica del CAB. Informe Técnico CNEA-CAB 89/045 (INIS 22:047191).

BALIÑO, J. L. & MENDIETA, H. 1989 Detector de flujo calórico crítico basado en el desbalance de resistencias. Informe Técnico CNEA-CAB 89/043 (INIS 22:047899).

BALIÑO, J. L. & CONVERTI, J. 1991 Critical heat flux in horizontal annular channels with variable eccentricity. *Int. Commun. Heat Mass Transfer* **18,** 659–667.

BALIÑO, J. L. 1991 Flujo calórico crítico en canales anulares horizontales excéntricos. Final Report to obtain the degree of Doctor in Nuclear Engineering, Instituto Balseiro, Argentina.

BAR-COHEN, A., RUDER, Z. & GRIFFITH, P. 1983 Circumferencial wall temperature variations in horizontal boiler tubes. *Int. J. Multiphase Flow* **9,** 1–12.

BENJAMIN, T. B. 1968 Gravity currents and related phenomena. *J. Fluid Mech.* **31,** 209–248.

BERGLES, A. E. 1977 Burnout in boiling heat transfer. Part II: subcooled and low-quality forced-convection systems. *Nucl. Safety* **18,** 154–167.

DUKLER, A. E. & HUBBARD, M. G. 1975 A model for gas-liquid slug flow in horizontal and near-horizontal tubes. *Ind. Engng Chem. Fundam.* **14,** 337–347.

DUKLER, A., MARON, D. M. & BRAUNER, N. 1985 A physical model for predicting the minimum stable slug length. *Chem. Engng Sci.* **40,** 1379–1385.

FIORI, M. P. & BERGLES, A. E. 1970 Model of critical heat flux in subcooled flow boiling. *Proc. 4th Int. Heat Transfer Conf.*, Versailles, Paper B6-3.

FISHER, S. A., HARRISON, G. S. & PEARCE, D. C. 1978 Premature dryout in conventional and nuclear power station evaporators. *Proc. 6th. Int. Heat Transfer Conf.*, Toronto, Vol. 2, pp. 49–54.

HASHIZUME, K. 1983 Flow pattern, void fraction and pressure drop of refrigerant two-phase flow in a horizontal pipe. *Int. J. Multiphase Flow* **9,** 399–410.

HEWITT, G. F. 1982 Burnout. In *Handbook of Multiphase Systems* (Edited by HETSRONI, G.), pp. 6.66–6.141. McGraw–Hill, New York.

KAYS, W. M. & CRAWFORD, M. E. 1980 *Convective Heat and Mass Transfer*, 2nd edn. McGraw–Hill, New York.

KEFER, V., KOHLER, W. & KASTNER, W. 1989 Critical heat flux (CHF) and post-CHF heat transfer in horizontal and inclined evaporator tubes. *Int. J. Multiphase Flow* **15,** 385–392.

KUTATELADZE, S. S. & LEONTIEV, A. I. 1966 Some applications of the asymptotic theory of the turbulent boundary layers. *Proc. 3rd Int. Heat Transfer Conf.*, Chicago, IL, Vol. 3, pp. 1–6.

KVERNVOLD, O., VIDNOY, B., SONTVED, T., SAASEN, A. & SELMER-OLSEN, S. 1984 Velocity distribution in horizontal slug flow. *Int. J. Multiphase Flow* **10,** 451–457.

LEVY, S., POLOMIK, E. E., SWAN, C. L. & MCKINNEY, A. W. 1962 Eccentric rod burnout at 1000 psia with net steam generation. *Int. J. Heat Mass Transfer* **5.**

MANDHANE, J. M., GREGORY, G. A. & AZIZ, K. 1974 A flow pattern map for gas–liquid flows in horizontal pipes. *Int. J. Multiphase Flow* **1,** 537–553.

MERILO, M. 1977 Critical heat flux experiments in a vertical and horizontal tube with both freon-12 and water as coolant. *Nucl. Engng Design* **44,** 1–16.

MERILO, M. & AHMAD, S. Y. 1979 The effect of diameter on vertical and horizontal flow boiling crisis in a tube cooled by freon-12. AECL 6485.

NICHOLSON, K. K., AZIZ, K. & GREGORY, G. A. 1978 Intermittent two-phase flow in horizontal pipes: predictive models. *Can. J. Chem. Engng* **56,** 653–663.

OSAMUSALI, S. I., GRENEVELD, D. C., SCHENK, J. R. & CHENG, S. C. 1991 A technique for non-visual characterization of two-phase flow patterns in a horizontal 37-rod bundle. *Proc. CNS Meeting.*

POTTER, M. C. & FOSS, J. F. 1975 *Fluid Mechanics*, pp. 340–341. Ronald Press, Oxford.

RUDER, Z., HANRATTY, P. J. & HANRATTY, T. J. 1989 Necessary conditions for the existence of stable slugs in horizontal pipes. *Int. J. Multiphase Flow* **15,** 209–226.

RUDER, Z. & HANRATTY, T. J. 1990 A definition of gas–liquid plug flow in horizontal pipes. *Int. J. Multiphase Flow* **16,** 233–242.

TAITEL, Y. & DUKLER, A. E. 1986 Flow pattern transition in gas–liquid systems: measurement and modelling. In *Multiphase Science and Technology* (Edited by HEWITT, G. F., DELHAYE, J. M. & ZUBER, N.), Vol. 2, pp. 1–94. Hemisphere, Washington, DC.

TOLUBINSKII, V. I. LITOSHENKO, A. K., DOMASHEV, E. D., KRAVCHENKO, A. S. & CHIROV, D. A. 1971 Critical heat transfer in eccentric annuli. *Teploenergetica* **18,** 64–66.

TONG, L. S. 1972 Boiling crisis and critical heat flux. USAEC Critical Review Series, Report TID-25887.

WONG, Y. L., GROENEVELD, D. C. & CHENG, S. C. 1990 CHF prediction for horizontal tubes. *Int. J. Multiphase Flow* **16,** 123–138.